Rev.Adv.Mater.Sci. 25 (2010) 155-163

DIAGNOSIS OF STRUCTURAL STATE OF BULK NANO- AND SUBMICROCRYSTALLINE SOFT MAGNETIC MATERIALS

N.I. Noskova and A.G. Lavrentiev

Institute of Metal Physics, Ural Branch RAS, 620041, S.Kovalevskay st. 18, Ekaterinburg, GSP-170, Russia

Received: October 01, 2009

Abstract. Different structural states - microcrystalline, submicrocrystalline, nanocrystalline (with a set of grain sizes each) and amorphous ones - of soft magnetic materials are considered. It is analyzed how the structural state of $Fe_5Co_{70}Si_{15}B_{10}$, $Fe_{60}Co_{20}Si_5B_{15}$, $Co_{81.5}Mo_{9.5}Zr_9$, and $Fe_{73.5-x}Co_xCu_1Nb_3Si_{13.5}B_9$ (x = 0, 10, 20, 30 at.%) amorphous alloys influences their magnetic characteristics in different nanocrystallization conditions. It is found that peculiarities of the fine structure and the grain size in the alloys under study correlate with their magnetic parameters and informative parameters of the Barkhausen effect in submicrocrystalline and nanocrystalline of soft magnetic materials.

1. INTRODUCTION

Magnetic properties of soft magnetic materials depend on their structural state, specific features of the domain structure, and stabilization of domain boundaries. Magnetic properties of ferromagnetic materials can be controlled by changing their structure. Structural parameters of alloys are altered using thermal (TT), thermomagnetic (TMT) and mechanical thermomagnetic (MTMT) treatments. The structure of amorphous nanocrystalline alloys after, e.g., TMT can be characterized by internal elastic distortions, pre-precipitates in the form of the amorphous matrix decomposition, the size of nanograins, and the chemical composition of nanoscale phases. The method of transmission electron microscopy is widely used for analysis of the structural state of amorphous and nanocrystalline alloys. Informative parameters of the Barkhausen effect [1,2] can provide additional information about the structure of polycrystalline alloys.

The present work deals with the influence of the structural state, which is established under different TT and TMT conditions in amorphous and nanocrystalline Fe- and Co-based alloys, on parameters of the Barkhausen effect.

2. EXPERIMENTAL

Amorphous ribbons were made by melt quenching on a rotating copper disk (ribbons 20-25 μm thick and 5 mm wide). The samples were shaped as strips and toroids. The study was performed taking samples of amorphous alloys having different values of the magnetostriction λ_s, such as $Fe_{60}Co_{20}Si_5B_{15}$ ($\lambda_s \sim 30\cdot10^{-6}$), $Fe_5Co_{70}Si_{15}B_{10}$ ($\lambda_s \sim 0.5\cdot10^{-6}$), $Fe_{73.5-x}Co_xCu_1Nb_3Si_{13.5}B_9$ ($\lambda_s \sim 0.2\cdot10^{-6}$) ($x$ = 0, 10, 20, 30 at.%) and $Co_{81.5}Mo_{9.5}Zr_9$ whose λ_s is

Corresponding author: N.I. Noskova, e-mail: noskova@imp.uran.ru

Table 1. Values of T_C and T_{cr} for amorphous and nanocrystalline alloys.

Alloy	T_C, °C	T_{cr}, °C
amorphous, $Fe_5Co_{70}Si_{15}B_{10}$	380	480
amorphous, $Fe_{60}Co_{20}Si_5B_{15}$	550	490
amorphous, $Co_{81.5}Mo_{9.5}Zr_9$	460	540
nanocrystalline, $Fe_{73.5}Cu_1Nb_3Si_{13.5}B_9$	570	540
amorphous, $Fe_{63.5}Co_{10}Cu_1Nb_3Si_{13.5}B_9$	480	490
amorphous, $Fe_{43.5}Co_{30}Cu_1Nb_3Si_{13.5}B_9$	420	490

almost zero. Quenching stresses were removed by annealing the samples in a vacuum at temperatures of 300 to 350 °C. Then the samples were subject to a thermal magnetic treatment in longitudinal magnetic fields of different frequencies (constant, alternating at f = 50 Hz, and high-frequency at f = 80 kHz fields) [3]. Some samples underwent a comprehensive thermal magnetic treatment which consisted in their annealing over some temperature interval and simultaneous application of (constant and high-frequency) magnetic fields. Some samples were quenched in an alternating magnetic field from the Curie temperature (the cooling rate was 5000 °/min).

The structure of amorphous ribbons was examined by the method of transmission electron microscopy in a JEM-200KX microscope. Foils, in which the thinnest regions were 200-300 nm thick, were made of the alloy ribbons by electrolytic polishing for observation in the electron microscope.

The EMF of a flux of Barkhausen jumps, e, averaged over the magnetization reversal time was taken as an informative parameter of the Barkhausen effect. The flux of Barkhausen jumps (BJ's) was visually observed on the oscilloscope screen. The EMF e was measured on strip samples using a lay-on sensor [4]. Static hysteresis loops, the initial magnetic permeability μ_0, and the magnetic loss $P_{0.2/20000}$ were measured for toroidal samples. The magnetic loss was measured at a frequency of 20 kHz and induction of 0.2 T. It was calculated from the surface area of dynamic hysteresis loops measured by the stroboscopic method. The initial magnetic permeability was determined at a frequency of 80 Hz in a field of 0.05 A/m. Static hysteresis loops were measured additionally for strip samples.

3. RESULTS AND DISCUSSION

Basic characteristics of the alloys, namely the Curie temperature T_C and the crystallization temperature T_{cr}, are given in Table 1. Table 2 presents magnetic properties of the $Fe_{60}Co_{20}Si_5B_{15}$, $Fe_5Co_{70}Si_{15}B_{10}$ and $Co_{81.5}Mo_{9.5}Zr_9$ alloys after thermal and thermomagnetic treatments in different conditions.

Fig. 1 shows hysteresis loops for the $Fe_5Co_{70}Si_{15}B_{10}$ alloy in different structural states: quick quenching on a rotating disk, annealing in the absence of a magnetic field, TMT in a constant magnetic field, and TMT in a high-frequency field (*f*

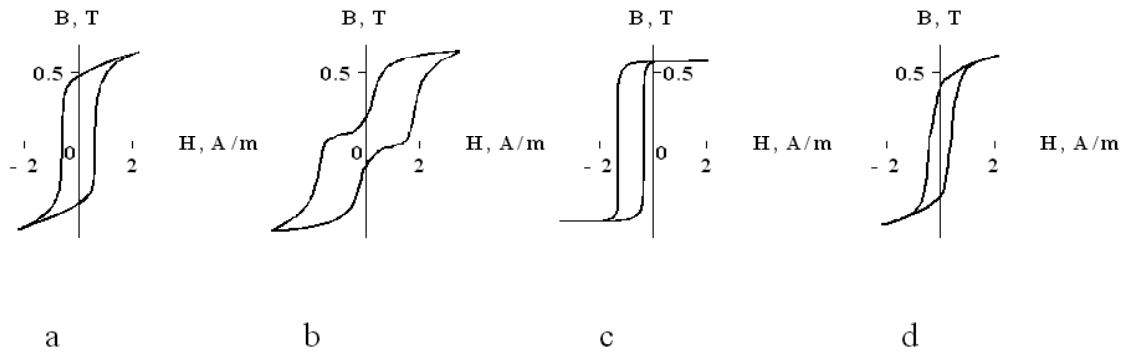

Fig. 1. Hysteresis loops for the $Fe_5Co_{70}Si_{15}B_{10}$ amorphous alloy subject to the following treatments: (a) – quick quenching; (b) – annealing in the absence of a magnetic field; (c) – TMT in a constant magnetic field; (d) – TMT in a high-frequency field [3].

Table 2. Magnetic properties of amorphous alloys after different treatments [3].

Alloy	*Treatment*	μ_o	H_c, A/m	$P_{0.2/20000}$, W/kg	B_r/B_m
$Fe_5Co_{70}Si_{15}B_{10}$	Annealing	4500	1.3	30	0.3
	TMT in a constant field	5200	0.6	37	0.97
	Quick cooling in an alternating field	45000	0.4	5	0.96
$Fe_{60}Co_{20}Si_5B_{15}$	Annealing	1050	2.5	55	0.3
	TMT in a constant field	1200	2.5	60	0.97
	Comprehensive TMT	7500	1.0	7	0.97
$Co_{81.5}Mo_{9.5}Zr_9$	Annealing	1200	1.5	35	0.4
	TMT in a constant field	3500	0.8	40	0.97
	Quick cooling in an alternating field	50000	0.3	5	0.96

= 80 kHz). The quickly quenched sample had a round symmetrical hysteresis loop. After annealing in the absence of a magnetic field the hysteresis loop was constricted. After TMT in a constant magnetic field the loop acquired a square shape, but was displaced on the *H* axis (ΔH). TMT in a magnetic field alternating at 80 kHz gave a round symmetrical hysteresis loop with the lowest coercive force. TMT in a high-frequency field was analogous to TMT in a rotating magnetic field. Notice that quenching of the $Fe_5Co_{70}Si_{15}B_{10}$ sample in water from the Curie temperature led to the same result as TMT in a high-frequency field. The uniaxial magnetic anisotropy caused by annealing in a constant or alternating magnetic field led to a highly rectangular hysteresis loop. Destabilization of the domain structure, which was due to the thermal treatment in a high-frequency magnetic field or quick cooling from the Curie temperature, resulted in symmetric hysteresis loops with a low coercive force.

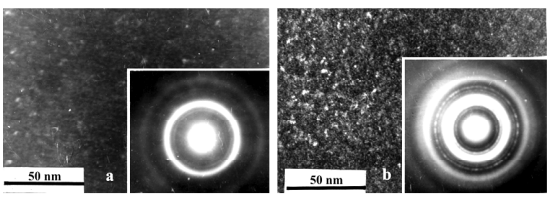

a b

Fig. 2. Dark-field electron microscopic images of the structure of the $Fe_5Co_{70}Si_{15}B_{10}$ amorphous alloy and a selected-area diffraction pattern after TMT in a constant field: (a) - TMT at 250 °C; (b) - TMT at 380 °C.

The hysteresis loops displaced along the field axis (ΔH), which were observed after TMT in a constant magnetic field, probably were due to the fact that the amorphous matrix contained high-coercivity microcrystalline precipitates whose magnetization direction depended on the direction of the magnetic field during TMT.

An examination of the structure of the $Fe_5Co_{70}Si_{15}B_{10}$ amorphous alloy showed that dispersed α-Co clusters appeared in the matrix of the amorphous sample after TMT in a constant magnetic field at 250 °C (ΔH was not over 1-2 H_c). The dark field image of the alloy structure after this treatment exhibits clusters in the form of sharp and blurred points. The internal ring is smeared in the selected-area diffraction pattern (Fig. 2a). After TMT in a constant magnetic field at a temperature of 380 °C (ΔH = 10-15 H_c) the alloy structure included dispersed precipitates (<5 nm in size) of the Co_2Si and Fe_3Si phases (Fig. 2b), which were not observed after low-temperature annealing. It may be concluded from the structural analysis that at TMT temperatures of 250-350 °C a small displacement of the hysteresis loop in the $Fe_5Co_{70}Si_{15}B_{10}$ amorphous alloy was caused mainly by α-Co clusters leading to stabilization of the domain structure. The displacement of the hysteresis loop in samples annealed at high temperatures probably was due to precipitation of dispersed phases having a higher coercive force.

Fig. 3 depicts hysteresis loops for the $Fe_{60}Co_{20}Si_5B_{15}$ amorphous alloy after melt quenching on a rotating disk, annealing in the absence of a magnetic field, TMT in a constant field, and after comprehensive TMT. It is seen that in the initial state (after melt quenching) the hysteresis loop was round

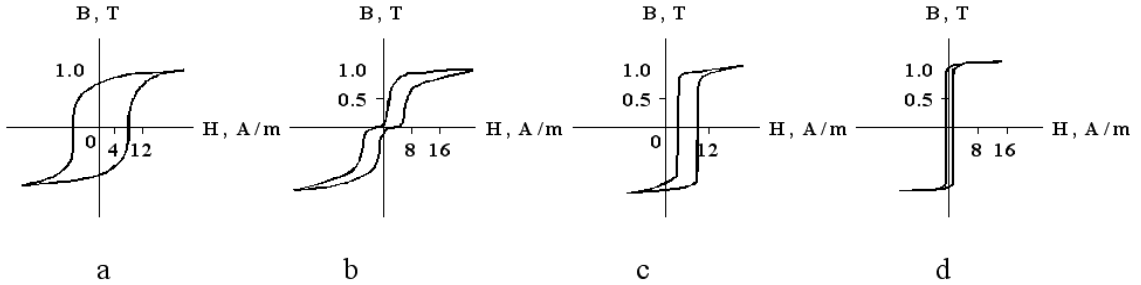

Fig. 3. Hysteresis loops for the $Fe_{60}Co_{20}Si_5B_{15}$ amorphous alloy after the following treatments: (a) quick quenching; (b) annealing in the absence of a magnetic field; (c) TMT in a constant magnetic field; (d) comprehensive TMT [3].

and symmetrical, with a high coercive force (H_c = 7 A/m). The sample had a large magnetic loss and a low initial magnetic permeability (see Table 2). Subsequent to annealing the hysteresis loop became constricted, with the constriction clearly defined. Annealing in a constant magnetic field led to a displaced hysteresis loop. In the case of comprehensive TMT the hysteresis loop became symmetrical, with a large squareness ratio (B_r/B_m = 0.95) and a low coercive force.

An analysis of the structure of the $Fe_{60}Co_{20}Si_5B_{15}$ alloy after TMT in a constant magnetic field at 400 °C revealed that the structure of this alloy had dispersed precipitates (<5 nm in size) of the Co_2Si and Fe_3Si phases (Fig. 4). The magnetization direction in these phases was determined by the direction of the magnetic field during TMT. Notice that this treatment caused a considerable displacement (ΔH ~ 10-15H_c) of the hysteresis loop in the alloy.

Fig. 5 shows oscillograms of amplitude envelopes of the BJ's flux in samples of the $Fe_{60}Co_{20}Si_5B_{15}$ alloy subject to annealing at 300 °C and TMT in a constant magnetic field at 400 °C. It is seen that BJ's had the Gaussian distribution in the field after annealing at 300 °C. After TMT in a constant field at 400 °C the oscillogram of the amplitude envelope of the BJ's flux exhibited several regions of critical start fields, and a shift along the field axis, which was caused by a displacement of the hysteresis loop, could be seen.

A comparison of the oscillograms showing the amplitude envelopes of the BJ's flux in Fig. 5 and the electron microscopic photographs of the structure of the $Fe_{60}Co_{20}Si_5B_{15}$ alloy in Fig. 4 suggested a correlation between the alloy structure and the chosen informative parameter of the Barkhausen effect: the Gaussian distribution of BJ's in the field corresponded to an amorphous structure, while the formation of dispersed precipitates in the alloy was

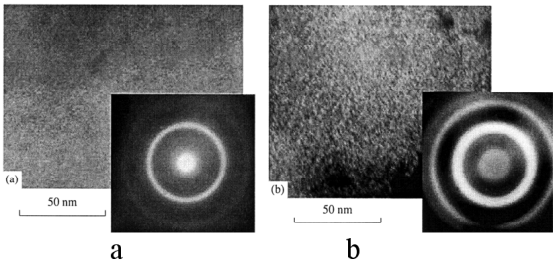

Fig. 4. Electron microscopic photographs of the structure of the $Fe_{60}Co_{20}Si_5B_{15}$ amorphous alloy and a selected-area diffraction pattern after the following treatments: (a) - thermal treatment at 300 °C, 1 hour; (b) - TMT in a constant field at 400 °C, 15 min.

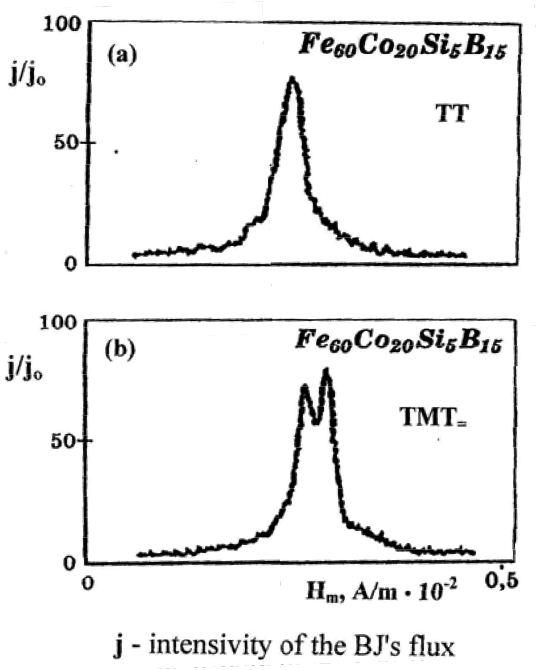

Fig. 5. Oscillograms of the amplitude envelopes of the BJ's flux in the $Fe_{60}Co_{20}Si_5B_{15}$ alloy after (a) thermal treatment at 300 °C for 1 hour and (b) TMT in a constant field at 400 °C for 15 min.

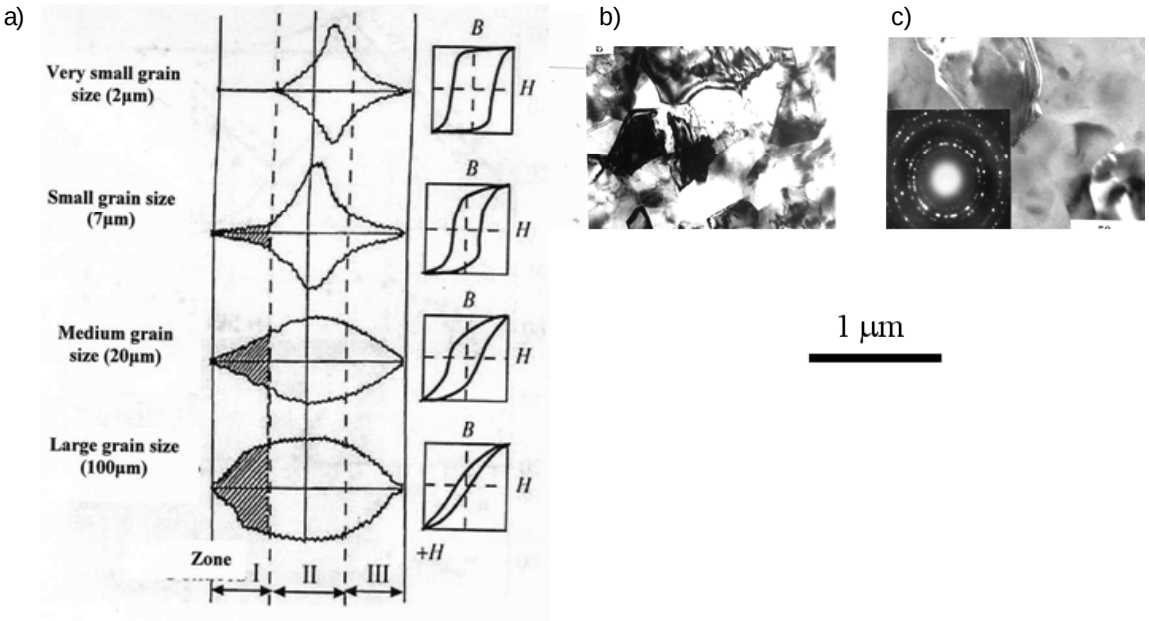

Fig. 6. Variation of the Barkhausen effect depending on the size of structure grains in the microcrystalline structural state (a) [5] and electron microscopic photographs of the structure with grains of the size d = 2 μm (b) and d = 20 μm (c).

followed by appearance of several regions of critical start fields in the oscillogram, which corresponded to precipitates in the amorphous matrix. The oscillogram of the BJ's flux amplitudes was not shifted along the field axis after TMT in an alternating magnetic field. The hysteresis loop became symmetrical. The amplitude of the jumps diminished. The region of critical start fields narrowed still more. The EMF of the BJ's flux, ε, after TMT in an alternating magnetic field was 8% lower than ε after TMT in a constant magnetic field. Notice that TMT in an alternating magnetic field led to a considerable increase in the initial magnetic permeability and a decrease in the magnetic loss.

It was shown earlier [5-7] that parameters of the Barkhausen effect in the microcrystalline structural state of alloys changed as fine (2 μm) grains were replaced by coarse (100 μm) ones (Fig. 6).

Results that differ from those of the studies [1,2,6] (Fig. 6) were also obtained for the $Co_{81.5}Mo_{9.5}Zr_9$ nonmetalloid alloy (see Table 2). Fig. 7 presents oscillograms of the amplitude envelopes of the BJ's flux for the $Co_{81.5}Mo_{9.5}Zr_9$ alloy (a) and electron microscopic photographs of its amorphous nanocrystalline structures (b, c, d) after different TT and TMT. At the same time, results obtained for this alloy almost replicated those for the $Fe_{60}Co_{20}Si_5B_{15}$ alloy (Fig. 5).

The effect of the annealing temperature of the $Fe_{73.5-x}Co_xCu_1Nb_3Si_{13.5}B_9$ alloys (x = 0, 10, 20, 30) on the coercive force was studied [4]. The relevant results are given in Table 3. The hysteresis loops for

Table 3. Effect of the annealing temperature of the $Fe_{73.5-x}Co_xCu_1Nb_3Si_{13.5}B_9$ alloy (x = 0, 10, 20, 30) on the coercive force H_c (A/m) [4] .

Annealing temperature, °C	*Co concentration, at.*%			
	0	10	20	30
	Coercive force, A/m /*Nanograin size*, nm			
350	12.7	0.40	0.24	3.2
400	10.3	0.24	0.16	1.6
450	3.2/6.5	0.32/2.5	0.16	0.8/3.5
500	0.56	0.40	0.24	2.2
540	0.64/10	0.48/8.0	0.56	32/15.0

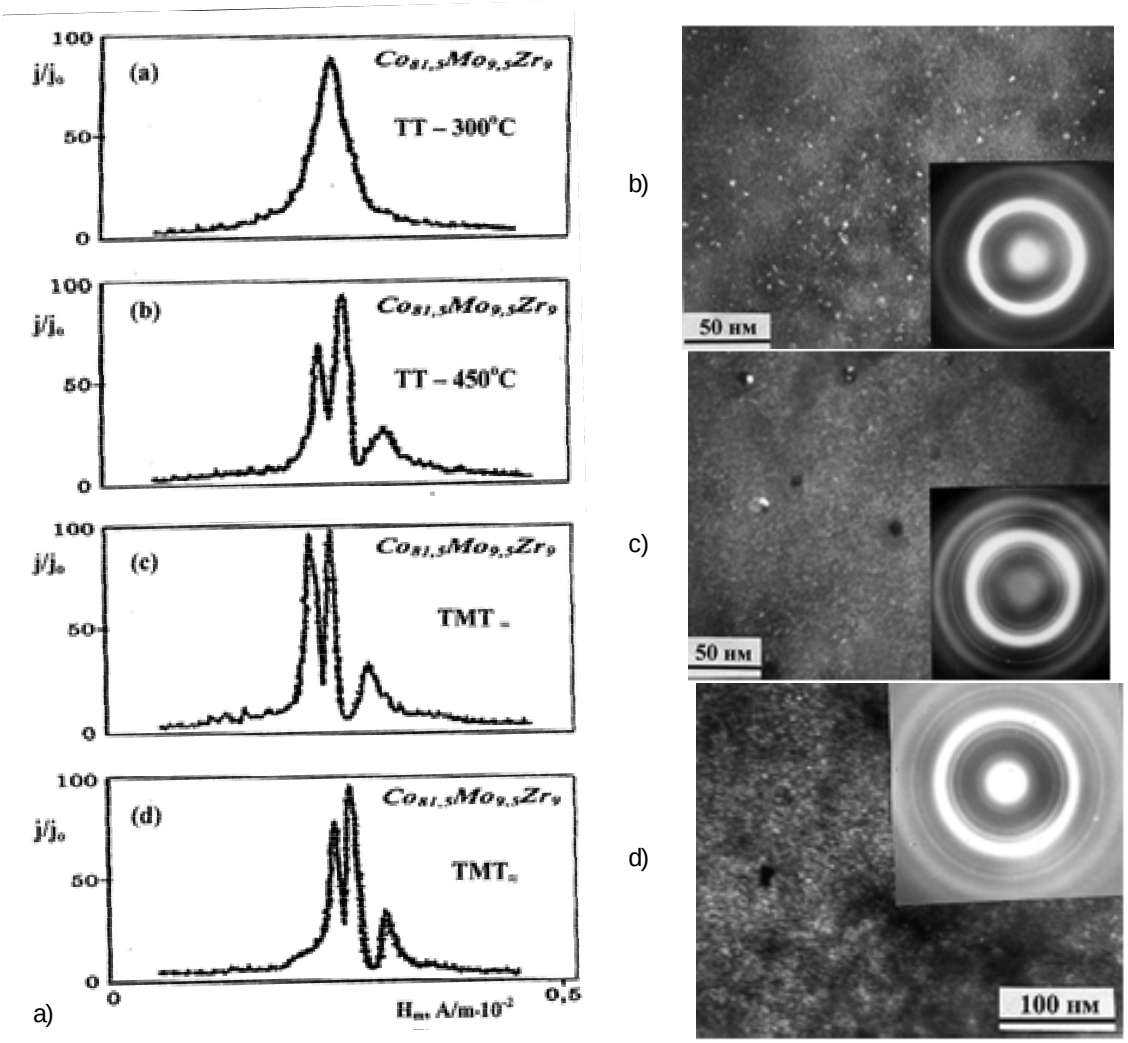

Fig. 7. Variation of the Barkhausen effect in amorphous nanocrystalline structural states (a) and electron microscopic photographs of the structure with selected-area diffraction patterns of the alloy after different TT and TMT: (b) - annealing at 300 °C, 2 h (α-Co and β-Co nanophases); (c) - TT at 450 °C, 1 h (α-Co, β-Co, and Co_2(Mo, Zr) nanophases); (d) - TMT in a constant magnetic field at 450°C, 1 h (α-Co, β-Co, and Co_2(Mo, Zr) nanophases) (the peaks reflect the presence of a nanophase-nanograins).

Table 4. Displacement field of the hysteresis loops (ΔH) depending on the composition of the $Fe_{73.5-x}Co_xCu_1Nb_3Si_{13.5}B_9$ alloy [4] .

Treatment	*x* (%)	0	10	20	30
TMT in a constant field	H_c, A/m	0.56	0.24	0.16	0.40
	ΔH, A/m	0	0.08	0.16	0.56
TMT in a high-frequency field	H_c, A/m	0.40	0.24	0.13	0.32
	ΔH, A/m	0	0	0	0

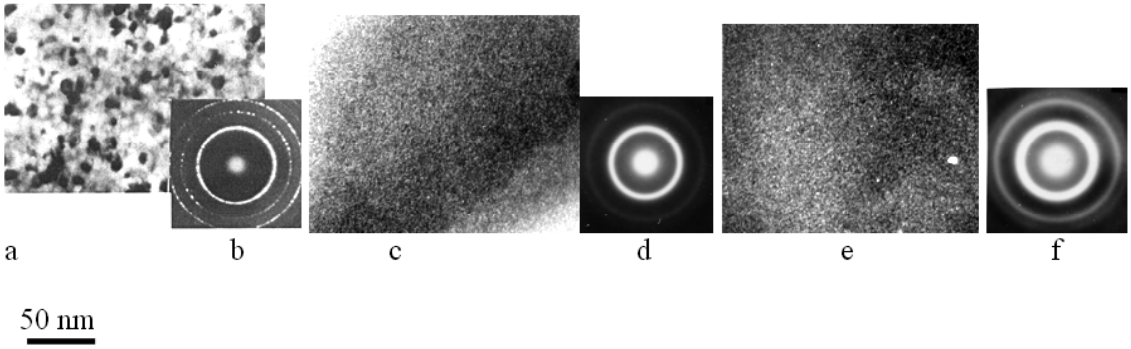

Fig. 8. Electron microscopic photographs of the structure (a, c, e) and selected-area diffraction patterns (b, d, f) of amorphous alloys: $Fe_{73.5}Cu_1Nb_3Si_{13.5}B_9$ after annealing at 520 °C for 2 h (a, b), $Fe_{63.5}Co_{10}Cu_1Nb_3Si_{13.5}B_9$ (c, d) and $Fe_{43.5}Co_{30}Cu_1Nb_3Si_{13.5}B_9$ (e, f) after annealing at 450 °C for 0.5 h.

the $Fe_{73.5-x}Co_xCu_1Nb_3Si_{13.5}B_9$ alloys annealed in the absence of a field were symmetrical at all values of *x*, while the displacement field of the hysteresis loop was zero. It is seen from Table 3 that the replacement of iron by cobalt at *x* = 10 and 20% Co and annealing at temperatures of 400-450 °C led to a considerable reduction of H_c probably because nanocrystallization of the alloy took place at lower temperatures and the saturation magnetostriction diminished. When *x* > 30 at. %, H_c increased.

Findings as to the effect of the substitution of Co for Fe atoms in the $Fe_{73.5-x}Co_xCu_1Nb_3Si_{13.5}B_9$ alloy (*x* = 10, 20, 30) on the displacement field of the hysteresis loop after TMT in a constant magnetic field are summarized in Table 4. It follows from Table 4 that TMT in a constant magnetic field increased the displacement field of hysteresis loops in the $Fe_{73.5-x}Co_xCu_1Nb_3Si_{13.5}B_9$ alloy with growing Co concentration.

The structure of the alloys with 0, 10, and 30 at.% Co was studied. The electron microscopic photographs in Fig. 8 show the structure of these alloys.

Figs. 8a-8f present electron microscopic photographs of the structure and selected-area diffraction patterns of the $Fe_{73.5}Cu_1Nb_3Si_{13.5}$ alloy annealed at 520 °C for 2 h and the $Fe_{63.55}Co_{10}Cu_1Nb_3Si_{13.5}B_9$ and $Fe_{43.5}Co_{30}Cu_1Nb_3Si_{13.5}B_9$ alloys annealed at 450°C for 0.5 h. It is seen from Fig. 8e that dispersed clusters of Co and Fe appeared in the matrix of the amorphous sample (“fine” points illuminate in the dark-field image taken with the iris aimed at the first halo, Fig. 8c).

The microstructure and selected-area diffraction patterns of the $Fe_{63.5}Co_{10}Cu_1Nb_3Si_{13.5}B_9$ and $Fe_{43.5}Co_{30}Cu_1Nb_3Si_{13.5}B_9$ amorphous nanocrystalline alloys annealed in a constant magnetic field at 450 °C are shown in Figs. 9a-9c, and 9d. The structure of the $Fe_{43.5}Co_{30}Cu_1Nb_3Si_{13.5}B_9$ alloy with a large Co concentration (Figs. 9c, 9d) changed considerably as compared to the structure of the $Fe_{63.5}Co_{10}Cu_1Nb_3Si_{13.5}B_9$ alloy after annealing in a

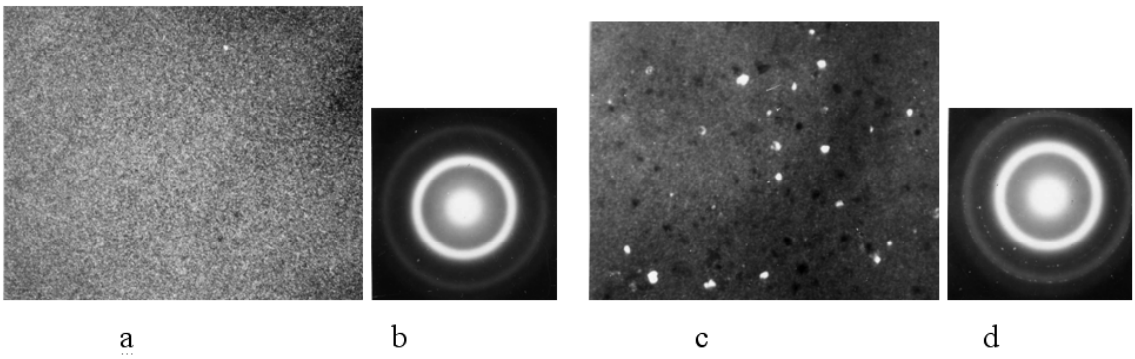

Fig. 9. Electron microscopic photographs of the structure (a, c) and selected-area diffraction patterns (b, d) of the $Fe_{63.5}Co_{10}Cu_1Nb_3Si_{13.5}B_9$ (a, b) and $Fe_{43.5}Co_{30}Cu_1Nb_3Si_{13.5}B_9$ (c, d) amorphous nanocrystalline alloys after TMT in a constant magnetic field.

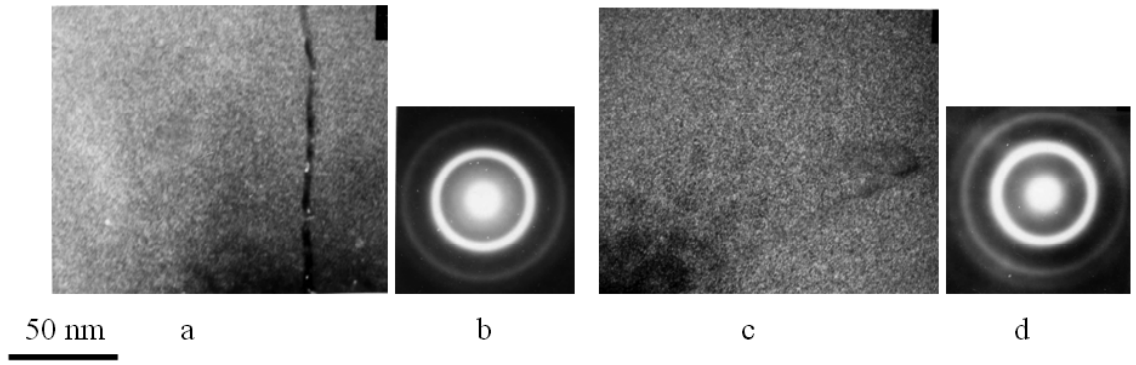

Fig. 10. Electron microscopic photographs of the structure (a, c) and selected-area diffraction patterns (b, d) of the $Fe_{63.5}Co_{10}Cu_1Nb_3Si_{13.5}B_9$ (a, b) and $Fe_{43.5}Co_{30}Cu_1Nb_3Si_{13.5}B_9$ (c, d) amorphous alloys after annealing at 450 °C for 0.5 h and TMT in an alternating magnetic field.

constant magnetic field at a temperature of 450 °C for 0.5 h. Annealing of the alloy with a large Co concentration at 450 °C was followed by precipitation, in addition to the formation of clusters, of hard magnetic $(Fe, Co)_3Si$ and $(Fe, Co)_2B$ nanophases having a high coercive force as compared to the corresponding force in alloys with a small Co concentration (Figs. 8c and 9a). Also, the matrix decomposed in alloys with $x > 30$ at.% considering that the first diffuse halo widened (Figs. 8f and 9d). A more intensive precipitation of these phases during TMT in a constant magnetic field probably led to an increase in the displacement field of the hysteresis loop.

The thermal magnetic treatment of $Fe_{73.5-x}Co_xCu_1Nb_3Si_{13.5}B_9$ amorphous nanocrystalline alloys in an alternating field ($f = 80$ kHz) led to symmetrical hysteresis loops, $\Delta H = 0$, at all values of x. This was probably due to the fact that in the case of TMT in a field alternating at 80 kHz the magnetization reversal in the samples was effected via the magnetization rotation process. When a sample was annealed in this field, the domain structure could not be fixed by vacancies, impurity atoms, clusters and other nanocrystalline precipitates on account of the absence of the preferential magnetization direction (the hysteresis loop became symmetrical, with a low coercive force). The microstructure and selected-area diffraction patterns of the $Fe_{73.5-x}Co_xCu_1Nb_3Si_{13.5}B_9$ amorphous nanocrystalline alloys ($x = 10, 30$) after TMT in an alternating field ($f = 80$ kHz) are shown in Figs. 10a-10d. It can be easily inferred from Figs. 10a and 10b that subsequent to TMT in an alternating magnetic field the alloy with 10% cobalt had an amorphous matrix, while the selected-area diffraction pattern contained a narrow halo. This observation points to relaxation processes resulting in a minimum concentration of defects that give rise to internal elastic stresses. It is seen from Fig. 10e that the alloy containing 30% Co had a structure characterized by a selected-area diffraction pattern with the first diffuse halo, which widened somewhat less than the diffuse halo in Fig. 8e. Therefore the concentration decomposition of the amorphous matrix of the alloy exposed to an alternating magnetic field can be assumed to be insignificant.

Thus, we demonstrated [7,8,9] that if the amorphous state undergoes devitrification and nanocrystallization, the Barkhausen effect also changes in a regular manner depending on the annealing temperature conditions used for precipitation of nanophases and formation of nanograins whose size can vary between 2 nm and 20 nm. This regular change consists in displacement and a different level of smearing of the peaks; two or even three peaks appear. It is different from the manner parameters of the Barkhausen effect change depending on the grain size in polycrystalline materials with coarse grains.

4. CONCLUSION

It is shown for the first time that parameters of the Barkhausen effect correlate with features of the fine structure at the initial stage of nanocrystallization of amorphous and amorphous nanocrystalline alloys, and they can be used to control the structural state of these alloys.

Considering the data on variation of the Barkhausen effect parameters depending on the

grain size in microcrystalline alloys, the obtained and available information regarding the change of the Barkhausen effect parameters can be recommended for diagnosing the scale of structural parameters in micro-, submicro-, and nanocrystalline alloys, and also amorphous materials.

A relationship between specific features of the fine structure of amorphous and amorphous nanocrystalline alloys at initial stages of nanocrystallization and the displacement field of the hysteresis loop in the alloys under study is established. It is shown that the magnetization reversal in samples subject to a thermomagnetic treatment in a constant magnetic field is accomplished due to a set of Barkhausen jumps with similar start fields, leading to an increase in the magnetic loss.

REFERENCES

[1] N.I. Noskova, V.V. Shulika, A.G. Lavrentiev, A.P. Potapov and G.S. Korzunin // *ZhTF* **75** (2005) 61.

[2] S. Tiitto // *Appl. Phys*. **119** (1977) 3.

[3] N.I. Noskova, V.V. Shulika, A.G. Lavrentiev, A.P. Potapov and G.S Korzunin // *J. FMM* **100 (**2005) 34.

[4] V.V. Shulika, A.P. Potapov and N.I. Noskova // *J. FMM* **104 (**2007) 241.

[5] E.S. Gorkunov, Yu.N. Dragoshanskii and M. Mikhovs // *Defektoskopiya* **8** (1999) 3, In Russian.

[6] E.S. Gorkunov, Yu.N, Dragoshanskii and M. Mikhovs // *Defektoskopiya* **6** (2000) 3, In Russian.

[7] E.S. Gorkunov, V.V. Shulika, A.G. Lavrentiev, A.P. Potapov and G.S. Korzunin // *Dokl. RAS* **386** (2002) 468.

[8] N.I. Noskova, V.V. Shulika, A.G. Lavrentiev, A.P. Potapov and G.S. Korzunin // *Defektoskopiya* **9** (2004) 63, In Russian.

[9] N.I.Noskova and R.R.Mulykov, *Submcrocrystallaine and nanocrystallaine metals and alloys* (Press UrB RAS, Ekaterinburg, 2003).